Beyond $Ti_3C_2T_x$: MXenes for Electromagnetic Interference Shielding

*Meikang Han[1], Christopher Eugene Shuck[1], Roman Rakhmanov[1, 2], David Parchment[1], Babak Anasori[1, 3], Chong Min Koo[4], Gary Friedman[2] and Yury Gogotsi[1]**

[1]A. J. Drexel Nanomaterials Institute and Department of Materials Science and Engineering, Drexel University, Philadelphia, PA 19104, USA

[2]Department of Electrical and Computer Engineering, Drexel University, Philadelphia, PA 19104, USA

[3]Department of Mechanical and Energy Engineering, Integrated Nanosystems Development Institute, Purdue School of Engineering and Technology, Indiana University–Purdue University Indianapolis, Indianapolis, IN 46202, USA

[4]Materials Architecturing Research Centre, Korea Institute of Science and Technology (KIST), Seoul 02792, Korea

* Corresponding author: Prof. Yury Gogotsi (Y. G.), E-mail: gogotsi@drexel.edu.

This is the author's manuscript of the article published in final edited form as:

Han, M., Shuck, C. E., Rakhmanov, R., Parchment, D., Anasori, B., Koo, C. M., ... & Gogotsi, Y. Beyond Ti3C2Tx: MXenes for Electromagnetic Interference Shielding. ACS Nano. https://doi.org/10.1021/acsnano.0c01312

ABSTRACT

New ultrathin and multifunctional electromagnetic interference (EMI) shielding materials are required for protecting electronics against electromagnetic pollution in the fifth-generation networks and Internet of Things era. Micrometer-thin $Ti_3C_2T_x$ MXene films have shown the best EMI shielding performance among synthetic materials so far. Yet, the effects of elemental composition, layer structure, and transition metal arrangement on EMI shielding properties of MXenes have not been explored, despite the fact that more than 30 different MXenes have been reported and many more are possible. Here, we report on a systematic study of EMI shielding properties of 16 different MXenes, which cover single-metal MXenes, ordered double-metal carbide MXenes, and random solid solution MXenes of M and X elements. This is the largest set of MXene compositions ever reported in a comparative study. Films with thicknesses ranging from nanometers to micrometers were produced by spin-casting, spray-coating, and vacuum-assisted filtration. All MXenes achieved effective EMI shielding (>20 dB) in micrometer-thick films. The EMI shielding effectiveness of sprayed $Ti_3C_2T_x$ film with a thickness of only ~40 nm reaches 21 dB. Adjustable EMI shielding properties were achieved in solid solution MXenes with different ratios of elements. A transfer matrix model was shown to fit EMI shielding data for highly conductive MXenes, but could not describe the behavior of materials with low conductivity. This work shows that many members of the large MXene family can be used for EMI shielding, contributing to designing ultrathin, flexible, and multifunctional EMI shielding films benefitting from specific characteristics of individual MXenes.

KEYWORDS: MXene, two-dimensional, electromagnetic interference shielding, conductivity, film

The arrival of commercial fifth generation (5G; 450 MHz—52 GHz) networks and a significant increase in the number of wireless Internet of Things (IoT) devices working across diverse frequency ranges made communication stability and security without electromagnetic interference (EMI) a critical requirement.[1] Specifically, for flexible wearable devices and miniaturized electronics with complex architectures, such as electronic skins, sensors, Bluetooth components, *etc*., it has become more challenging to confront the selective jamming in different frequency ranges.[2]

Conventional metals (Ag, Cu, Ni, and others) provide excellent barriers against electromagnetic waves, but metal foils cannot be used in tiny microelectronic devices and deposition of thin metal films onto uneven device surfaces is not an easy task.[3,4] In addition, EMI shielding effectiveness (SE) of metal coatings is limited by the skin depths of metals, decreasing efficiency of ultrathin metal coatings and limiting their use in wearable and portable electronic devices.[5] Graphene, which has low density, high strength, and excellent chemical stability, was considered until recently as the most promising alternative to replace metals for EMI shielding.[6,7] In 2016, $Ti_3C_2T_x$ (T_x represents the surface termination groups) MXene films were demonstrated to have outstanding EMI shielding capability at micrometer-scale thickness, outperforming both metals and carbon materials (graphene, carbon nanotubes and carbon fibers).[8] Since then, tremendous efforts focused on optimizing the EMI shielding performance of $Ti_3C_2T_x$ and manufacturing of $Ti_3C_2T_x$ aerogels, $Ti_3C_2T_x$/polymer composites, and $Ti_3C_2T_x$/carbon hybrids.[9-14] MXenes are produced by a scalable selective etching in acidic solutions, that leads to -O, -OH and -F surface terminations making them solution-processable and available for various coating manufacturing techniques, including spray-coating, spin-casting, inkjet printing, dip-coating and interfacial assembly.[15-18] In addition, these functionalized surfaces facilitate adhesion and

bonding to substrates. All the above advantages indicate that MXene is an alternative to the conventional metals and carbon materials for EMI shielding. However, few studies have explored the EMI shielding properties of MXenes other than $Ti_3C_2T_x$, although more than 30 kinds of MXenes with different compositions and structures have been published.[19]

MXenes are typically synthesized from MAX phases, which have the general formula $M_{n+1}AX_n$ (n=1-4).[20] There are three common MAX phase structures, M_2AX, M_3AX_2 and M_4AX_3, where M represents the early transition metal, A is an A-group element of group 13 to 15 of the periodic table, and X is carbon and/or nitrogen.[21,22] Consequently, MXenes commonly have three structures: M_2XT_x, $M_3X_2T_x$ and $M_4X_3T_x$, as shown in **Figure 1**. Based on the different M and X elements, they can also be sorted as mono-metal MXenes, double-metal (M′ and M″) MXenes, and double-X (C and N - carbonitrides) solid solution MXenes. Double-metal MXenes exist in two different forms, depending on the distribution of M′ and M″ metals: 1) solid solution MXenes where the M-sites are randomly occupied by two kinds of metal atoms and 2) ordered MXenes where the M′ and M″ elements are separated into different layers (Figure 1). To date, most MXenes show active surfaces and good dispersion in water and some organic solvents due to the acid-etching process.[23] Therefore, the MXene family is a promising platform for multifunctional EMI shielding coatings/devices.

Despite the fact that the EMI shielding properties of $Ti_3C_2T_x$ have been explored extensively, little is known about the effects of layer structure, elemental composition, or metal element arrangement on EMI shielding performance. Here, we synthesized 16 different MXenes, comprising various elemental compositions and structures that include the three primary classes of MXenes, including mono-metal MXenes, ordered double-metal MXenes, and random solid

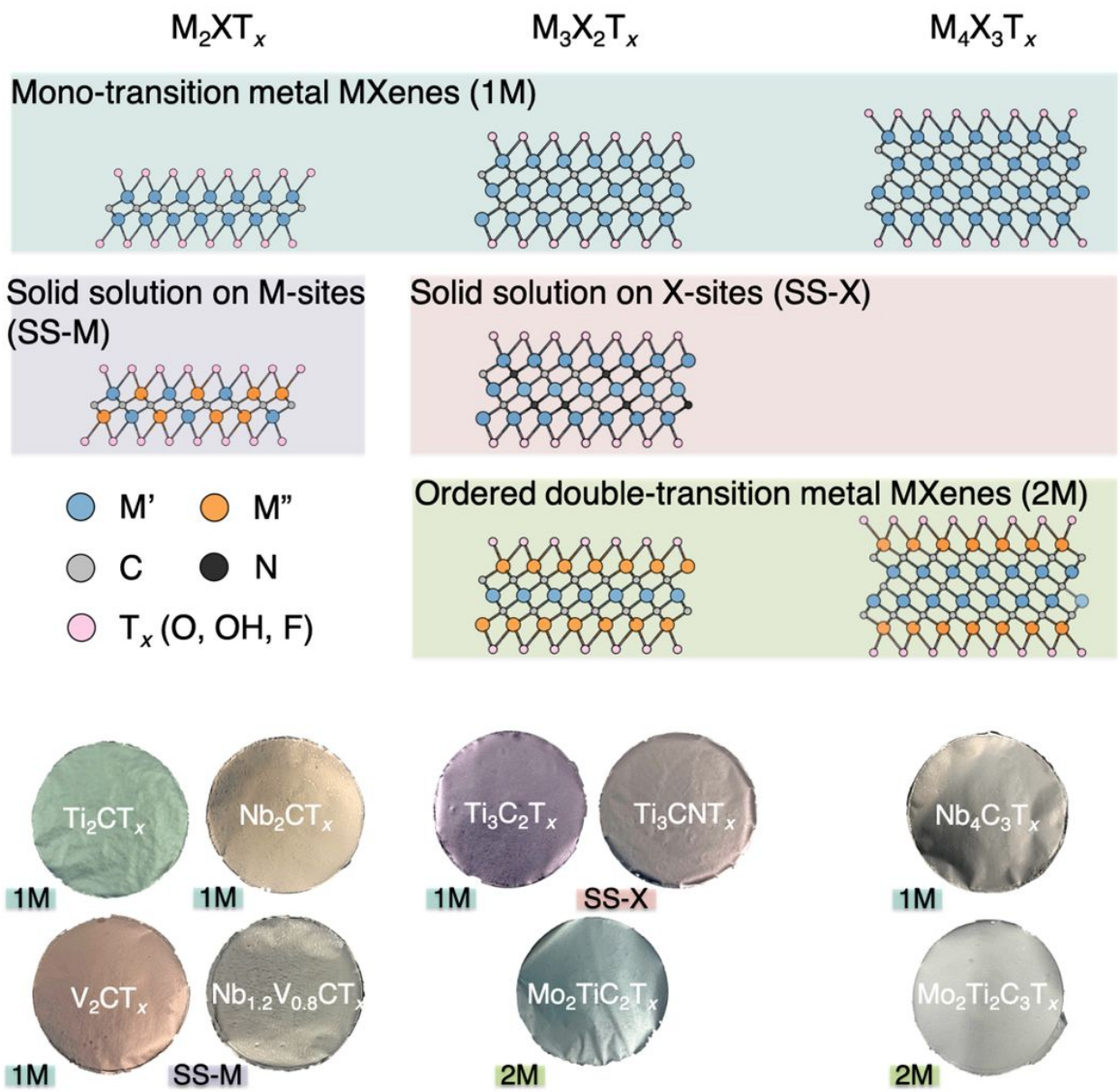

Figure 1. MXenes synthesized in this work. Atomic structures viewed from the [110] zone axis for three types of MXenes (M_2XT_x, $M_3X_2T_x$ and $M_4X_3T_x$, where T is shown as a bridging oxygen on the surface). They also can be sorted into four different kinds: mono-transition metal MXenes (1M), solid solution on M-sites (SS-M), solid solution on X-sites (SS-X (C and N)), and ordered double-transition metal MXenes (2M). Digital images of vacuum-filtrated freestanding films from different MXene colloidal solutions. '1M' MXene films: M_2CT_x (Ti_2CT_x, Nb_2CT_x and V_2CT_x), $Ti_3C_2T_x$, and $Nb_4C_3T_x$; SS-M MXene films: $Ti_yNb_{2-y}CT_x$ and $Nb_yV_{2-y}CT_x$ (y = 0.4, 0.8, 1.2 and 1.6); eight solid solutions on M-sites MXenes with different ratios of metal elements were synthesized in this work, here $Nb_{1.2}V_{0.8}CT_x$ film is as an example; '2M' MXene films: $Mo_2TiC_2T_x$ and $Mo_2Ti_2C_3T_x$; 'SS-X' MXene film: Ti_3CNT_x. The film diameter is 47 mm.

solution MXenes (Figure 1). The EMI shielding performance of MXene films with the thicknesses from nano to microscale has been investigated. Fitting of the results for different MXenes with a transfer matrix model provides some insights into the relationships between their EMI shielding properties and frequency/thickness/electrical conductivity. The produced very large set of EMI shielding capability data for the MXene family enables the rational design of EMI shielding coatings using different MXenes.

RESULTS AND DISCUSSION

Sixteen different MAX phases, including mono-M (Ti_2AlC_2, V_2AlC_2, and Nb_2AlC_2) and solid solution M_2AX ($Ti_yNb_{2-y}AlC$ and $Nb_yV_{2-y}AlC$ (y = 0.4, 0.8, 1.2 and 1.6)), M_3AX_2 (Ti_3AlC_2, Ti_3AlCN and Mo_2TiAlC_2), and M_4AX_3 (Nb_4AlC_3 and $Mo_2Ti_2AlC_2$), were initially synthesized. All synthesis conditions were summarized in Table S1. X-ray diffraction (XRD) patterns of all MAX phases are shown in Figure S2. Correspondingly, 16 different MXenes were obtained by the selective removal of the Al layers from MAX phase precursors using different etching and delamination processes. Figure 1 shows the freestanding MXene films prepared *via* vacuum-assisted filtration from the colloidal MXene solutions. MXenes have widely differing optical properties, which can be visually observed in the freestanding films.[17,24] These films represent the primary MXene categories: A) mono-M MXenes. Ti_2CT_x (green), Nb_2CT_x (gold), V_2CT_x (bronze), $Ti_3C_2T_x$ (purple) and $Nb_4C_3T_x$ (dark grey); B) double-X MXene. Ti_3CNT_x (violet black); C) double-M MXenes. $Mo_2TiC_2T_x$ (silver grey), $Mo_2Ti_2C_3T_x$ (silver), $Ti_yNb_{2-y}CT_x$ and $Nb_yV_{2-y}CT_x$. Of these, $Mo_2TiC_2T_x$ and $Mo_2Ti_2C_3T_x$ are ordered with the arrangement of Mo-Ti-Mo and Mo-Ti-Ti-Mo, respectively.[25] $Ti_yNb_{2-y}CT_x$ and $Nb_yV_{2-y}CT_x$ are random solid solutions whose colors change based on their specific chemical compositions. All the elemental

ratios for $Ti_yNb_{2-y}CT_x$ and $Nb_yV_{2-y}CT_x$ are based on compositions of solid solution MAX phases, assuming no transition metal loss during etching. Complete delamination of all MXenes was confirmed by XRD patterns of the MXene films (Figure S3). All of them show a prominent (002) diffraction peak of MXene at 2θ = ~5.3-7.3°. For all systems where the MAX is converted to MXene, the Al layer is removed, and replaced with the surface terminations, in addition to water and intercalants between the layers, leading to enlarged *d*-spacing compared to MAX phase precursors.[26] Hence, the observed *d*-spacing values are related to both the thickness of the MXene flakes (*n*) and the intercalants. For example, the (002) peaks *d*-spacing of Ti_2AlC, Ti_3AlC_2, and Nb_4AlC_3 is 6.7 Å (2θ = 13.1°), 9.2 Å (2θ = 9.60°), and 12.0 Å (2θ = 7.36°), respectively. After conversion of these MAX phases into MXenes, the (002) peak *d*-spacing of Ti_2CT_x, $Ti_3C_2T_x$, and $Nb_4C_3T_x$ increased to 12.1 Å (2θ = 7.28°), 12.6 Å (2θ = 7.00°), and 16.6 Å (2θ = 5.32°), respectively. The *d*-spacing expansion from M_2XT_x, $M_3X_2T_x$ to $M_4X_3T_x$ can be due to the presence of intercalants, such as TMAOH, used to delaminate MXene, and water molecules.

To investigate the EMI shielding performance of different MXenes, spin-casting, spray-coating, and vacuum-assisted filtration were used to fabricate MXene films of various thickness. For MXene films with a thickness of ~2 nm, we used a 130 μm-thick glass slide with negligible EMI SE as substrate (Figure S4), and deposited Ti_2CT_x and $Ti_3C_2T_x$ films by spin-casting. Spray-coating was used to fabricate < 150 nm Ti_2CT_x and $Ti_3C_2T_x$ films. Using vacuum-assisted filtration of the colloidal MXene solutions, ~1-15 μm thick MXene films were prepared. All vacuum-filtered MXene films were freestanding and flexible, which is attributed to the 2D morphology of the delaminated MXene flakes (Figure 2a, b). All MXenes investigated here have similar 2D morphologies with varying lateral dimensions. As an example, Ti_2CT_x flakes and

films are presented in Figure 2a-d. Both spray-coated films and filtered films show a similar aligned layered structure in cross-section (Figures 2c and 2d). It is noteworthy that the spray-coated films have better (more planar) stacking order than the filtered films owing to the layer-by-layer drying process. This was further confirmed by surface roughness analysis of spin-cast and spray-coated films using optical and SEM images (Figure S5). The density of spray-coated $Ti_3C_2T_x$ films was ~3.8 g cm^{-3} while that of filtered $Ti_3C_2T_x$ films was ~2.7 g cm^{-3}. The more uniform stacked layers lead to a higher film density (better interflake contact), which results in a higher electrical conductivity.

Figures 2e-g show the total EMI SE (SE_T) values for all MXene films of similar thicknesses (5 ± 0.3 μm) in the X-band (8.2-12.4 GHz). All exhibit a quasilinear frequency-dependent behavior whereby the SE_T decreases with increasing frequency. This indicates that all studied MXenes have a similar frequency-dependent conductive behavior. When the film thickness is ~5 μm, the total EMI SE values of all MXenes, except Nb_2CT_x and $Mo_2TiC_2T_x$, exceed 20 dB which means > 99% shielding efficiency in the whole X-band (Figure 2e). It was observed that Ti-based MXenes (Ti_2CT_x, Ti_3CNT_x, and $Ti_3C_2T_x$) with SE_T values above 40 dB have better EMI shielding performance than other MXenes. In particular, the performance of solid-solution MXenes ($Ti_yNb_{2-y}CT_x$ and $Nb_yV_{2-y}CT_x$) was compared with mono-M M_2CT_x MXenes (Ti_2CT_x, Nb_2CT_x, and V_2CT_x), as shown in Figure 2f, g. For $Ti_yNb_{2-y}CT_x$, their SE_T values are between Ti_2CT_x and Nb_2CT_x, and increase with the atomic ratio of Ti. Similarly, the SE_T values of $Nb_yV_{2-y}CT_x$ increase with the amount of V. These trends indicate that the EMI shielding properties of solid-solution MXenes are tunable by controlling of the M′/M″ ratios. We further studied the reflection and absorption behavior of different MXenes. The average EMI SE

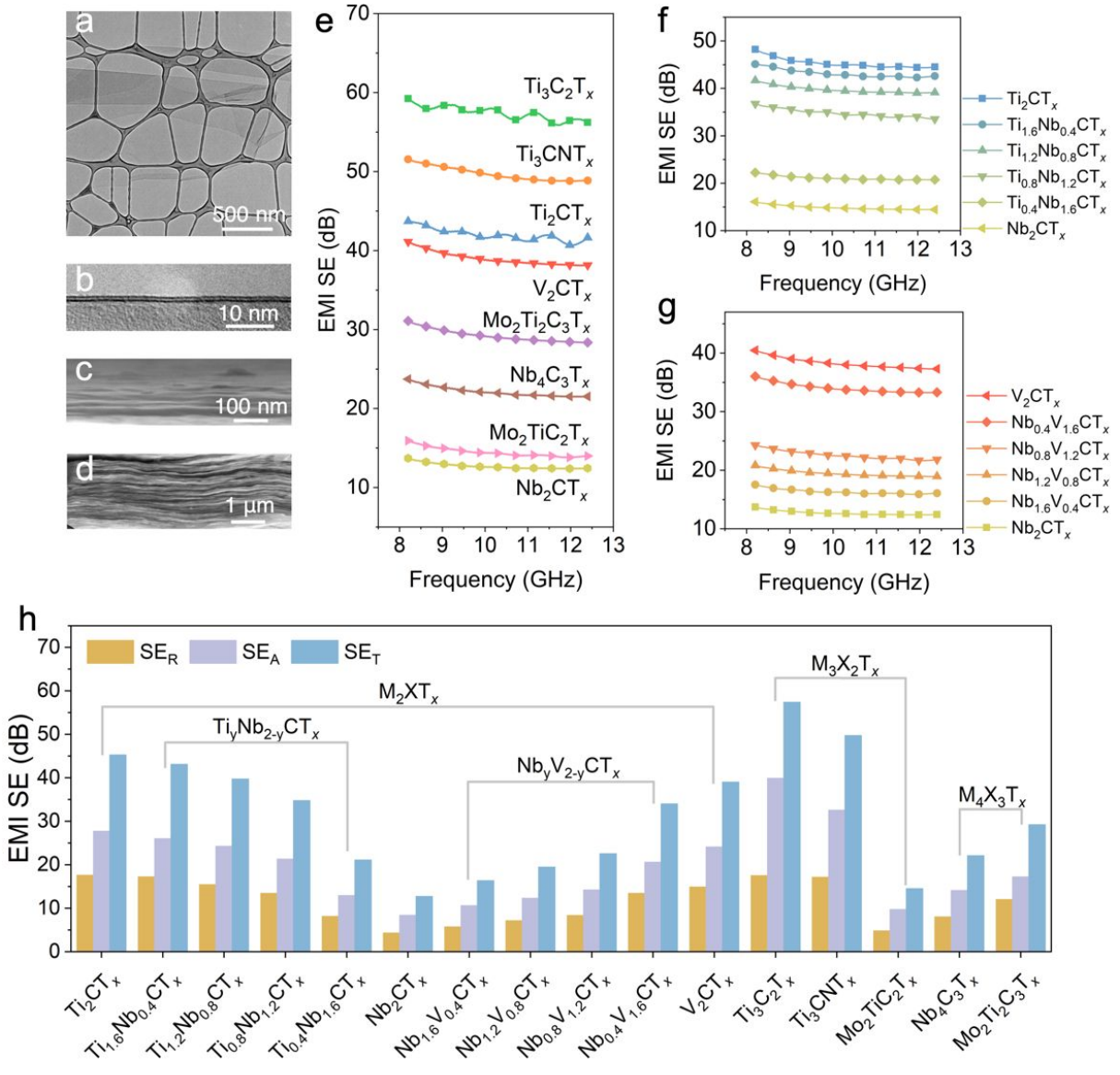

Figure 2. Frequency-dependent EMI shielding performance of different MXenes. (a) In-plane ([002] zone axis) TEM image of a typical MXene flake (Ti_2CT_x as an example). (b) TEM image of a double-layer MXene flake. (c) SEM image of the cross-section of a spray-coated Ti_2CT_x film on glass substrate showing an aligned layered structure. (d) SEM image of the cross-section of a vacuum-filtered freestanding Ti_2CT_x film showing the well-aligned layers. (e) EMI shielding effectiveness of different MXene (M_2XT_x, $M_3X_2T_x$ and $M_4X_3T_x$) films (5 ± 0.3 μm thick) in 8.2-12.4 GHz. EMI shielding effectiveness of solid solution (f) $Ti_yNb_{2-y}CT_x$ and (g) $Nb_yV_{2-y}CT_x$ MXene films (5 ± 0.3 μm thick), showing the controllable change of EMI SE with the chemistry. (h) The average EMI SE (SE_R, SE_A and SE_T) of different MXene films (5 ± 0.3 μm thick) in 8.2-12.4 GHz, showing the reflection and absorption contributions.

(SE_T, SE_R and SE_A) values in the X-band for different MXenes with a similar thickness (5 ± 0.3 μm) is shown in Figure 2h. MXenes with higher SE_T exhibit higher SE_R and SE_A values simultaneously, indicating that MXenes with higher EMI shielding capability have a higher contribution from EM wave reflection. Typically, the SE_T, SE_R and SE_A values for $Ti_yNb_{2-y}CT_x$ and $Nb_yV_{2-y}CT_x$ decrease with increasing amounts of Nb. For $M_3X_2T_x$ MXenes, the average SE_T, SE_R and SE_A of $Ti_3C_2T_x$ reach 57.4 dB, 17.5 dB and 39.9 dB, respectively, while Ti_3CNT_x values are 49.7 dB, 17 dB and 32.7 dB, respectively. We synthesized $Ti_3C_2T_x$ and Ti_3CNT_x using the same etching (HF and HCl) and delamination (LiCl) methods. It suggests that the mono-X MXene has better EMI shielding performance than the double-X MXene (carbonitride). For ordered double-M MXene, $Mo_2TiC_2T_x$, whose outer metal layers are Mo, shows a much lower EMI shielding capability, in comparison with $Ti_3C_2T_x$.

Because EMI shielding properties are sensitive to the thickness of the shielding layers, we measured the EMI shielding performance of all MXene films over a wide range of thicknesses, and applied a model based on the transfer matrix method to validate them. Figure 3a illustrates the continuum multi-layer structure with a plane EM wave (far-field) at normal incidence to single MXene layers with interlayered free space (details of calculations are presented in Supporting Information). Generally, Simon's formula is the most common approach to verify the EMI shielding performance for highly conductive materials with thicknesses above the skin depth ($d \gg \delta$).[27] However, it is not applicable to nanometer- and submicrometer-thick MXene films. The advantage of the transfer matrix modeling for ultrathin shielding layers, compared to Simon's formula that neglects multiple reflection between the layers, is shown in Figure S1. In absence of a model capturing the physics behind interactions of atomically thin materials and EM waves[28], this looks like the best option available today.

Figure 3b shows typical nanometer-thick $Ti_3C_2T_x$ (dark green) and Ti_2CT_x (dark purple) films fabricated by spray-coating, and transparent single-layer MXene films that were spin-cast on glass substrates. The thickness of single-layer $Ti_3C_2T_x$ and Ti_2CT_x flakes was measured using atomic force microscopy (AFM, Figure S6). The film thickness was calculated based on the transmittance and the absorption coefficients of $Ti_3C_2T_x$ and Ti_2CT_x films at 550 nm wavelength (details in Figure S7).[29,30] The visible transmittance and color change with the increasing film thickness of $Ti_3C_2T_x$ and Ti_2CT_x films are shown in Figure S8. Figure 3c shows the EMI SE_T values of various nanometers-thick $Ti_3C_2T_x$ and Ti_2CT_x films at 10 GHz. As the $Ti_3C_2T_x$ films thickness increases from ~2 nm to 137 nm, the SE_T value increases from 1.4 dB to 33 dB. It is highly significant that at ~40 nm film thickness, the SE_T value reaches 21 dB, indicating that more than 99% of the EM waves have been intercepted. For Ti_2CT_x films, at 94 nm film thickness, the SE_T value reaches 13 dB, which is equivalent in shielding to a ~14 nm-thick $Ti_3C_2T_x$ film. The gray line shows the simulated results using the transfer matrix model with the electrical conductivity. The modelling results agree sufficiently well with the experimental data. The SE_T values of $Ti_3C_2T_x$ and Ti_2CT_x films decrease with the increasing frequency in the X-band (Figure S9a, b). Both SE_A and SE_R values increase with the increasing thickness (Figure S9c, d).

We further measured the total EMI SE values of all the vacuum-filtered MXene films with thicknesses ranging from ~1 to 15 μm. As shown in Figure 3d, the SE_T values of all the films show a nonlinear monotonic increase with the thickness, in fairly good agreement with the simulated results from the electrical conductivity values (gray line). This statistical result demonstrates that the transfer matrix model is more suitable for predicting the EMI shielding properties of thin films, as opposed to Simon's formula which predicts a linear relationship

between thickness and EMI SE. Significantly, except Nb_2CT_x, all studied MXene films achieved SE_T > 20 dB below 10 μm thickness, including M_2XT_x (Ti_2CT_x and V_2CT_x), $M_3X_2T_x$ ($Ti_3C_2T_x$, Ti_3CNT_x and $Mo_2TiC_2T_x$), and $M_4X_3T_x$ ($Nb_4C_3T_x$ and $Mo_2Ti_2C_3T_x$). In particular, $Ti_3C_2T_x$, Ti_3CNT_x, Ti_2CT_x, V_2CT_x and $Mo_2Ti_2C_3T_x$ films show SE_T > 20 dB below 2.5 μm film thickness. Compared to Nb_2CT_x, $Nb_4C_3T_x$ which has a similar elemental composition, shows a higher EMI SE at all film thicknesses. The same trend was found for Ti_2CT_x and $Ti_3C_2T_x$. It indicates that higher conductivity and EMI shielding can be obtained by increasing the number of layers in the

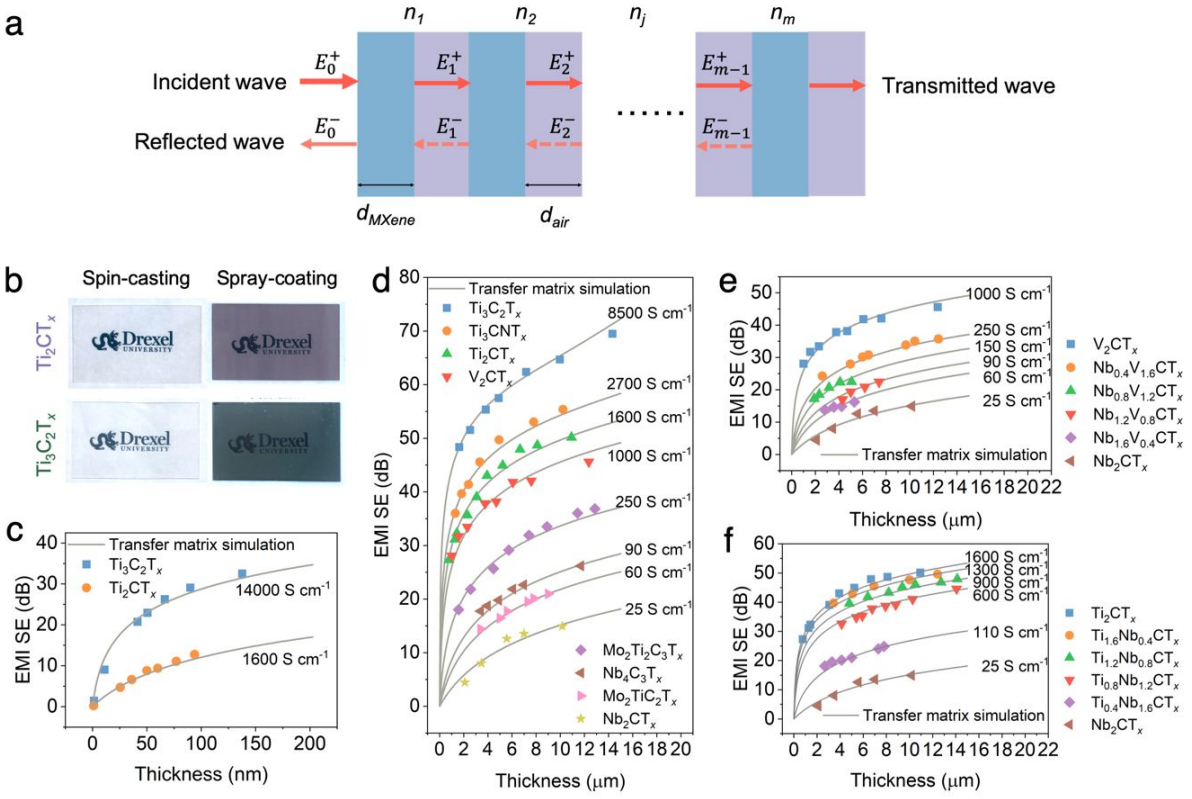

Figure 3. **Thickness-dependent EMI shielding performance of different MXenes.** (a) Schematic illustration for transfer matrix model simulating the interaction between the incident EM wave and MXene layers at normal incidence. (b) Digital images of spin-cast single-layer MXene films ($Ti_3C_2T_x$ and Ti_2CT_x), and spray-coated MXene films on glass substrates. (c) Simulated and experimental EMI SE values of spin-cast and spray-coated films ($Ti_3C_2T_x$ and Ti_2CT_x) with different thicknesses (<150 nm) at 10 GHz. (d) Simulated and experimental EMI SE values of vacuum-filtered MXene (M_2XT_x, $M_3X_2T_x$ and $M_4X_3T_x$) films with thicknesses from ~1 to 15 μm at 10 GHz. Simulated and experimental EMI SE values of solid solution (e) $Nb_yV_{2-y}CT_x$ and (f) $Ti_yNb_{2-y}CT_x$ MXene films with different thicknesses at 10 GHz. The electrical conductivity values for the simulation are listed (c, d, e, and f).

MXene structure. The EMI shielding properties of two kinds of solid solution MXenes ($Nb_yV_{2-y}CT_x$ and $Ti_yNb_{2-y}CT_x$) were also measured and modeled at different thicknesses. Compared to pure Ti_2CT_x, V_2CT_x and Nb_2CT_x, the SE_T values of $Nb_yV_{2-y}CT_x$ monotonically increase with the V content, likewise with $Ti_yNb_{2-y}CT_x$ and Ti content (Figure 3e, f). Additionally, both show excellent EMI shielding capabilities; $Ti_yNb_{2-y}CT_x$ and $Nb_yV_{2-y}CT_x$ films can achieve $SE_T > 20$ dB below 4 μm and 8 μm film thicknesses, respectively. This suggests that, in addition to $Ti_3C_2T_x$, many other MXenes can be used as thin EMI shielding coatings, although the performance of $Ti_3C_2T_x$ is still the best, possibly due to the optimized synthesis process that minimized the concentration of defects and maximized the conductivity compared to initial reports.[13,14] This is important as MXenes offer a variety of colors, mechanical, electrical and other properties, enabling development of multifunctional EMI shielding films and coatings. Furthermore, the EMI shielding performance is demonstrated to be tunable by control of the chemistry of solid-solution MXenes over a broad range of thicknesses and compositions. The frequency-dependent EMI SE values of all MXene films with different thicknesses can be found in Figure S10. Notably, the electrical conductivity of the sprayed $Ti_3C_2T_x$ films is ~14000 S cm^{-1}, compared to the vacuum-filtered films (~8500 S cm^{-1}). This is attributed to better alignment and denser packing of MXene layers in the sprayed films (Figure S5).

To further understand the correlation between the electrical conductivity and EMI SE of MXene films, we measured the electrical conductivity of all vacuum-filtered MXene films using the four-point probe method. As shown in Figure 4a, Ti-based MXenes ($Ti_3C_2T_x$, Ti_3CNT_x, Ti_2CT_x, and $Ti_{1.6}Nb_{0.4}CT_x$) along with V_2CT_x, exhibit electrical conductivity higher than 1000 S cm^{-1}, while Nb-based MXenes have relatively low electrical conductivity. It is noteworthy that the conductivity of MXenes varies with different synthesis processes and precursors. For the

solid solution MXenes studied, the electrical conductivity of $Ti_yNb_{2-y}CT_x$ and $Nb_yV_{2-y}CT_x$ films decreases with the increasing Nb content, consistent with the change of EMI shielding performance. This indicates that both the electrical conductivity and EMI shielding capability of MXenes are adjustable *via* their chemical composition.

We further simulated the total EMI SE of MXene films with a thickness of 5 μm using the transfer matrix modeling at frequency of 10 GHz, and compared the modeled values to experimentally measured electrical conductivity and SE_T. As shown in Figure 4b, for MXenes with an electrical conductivity of > 100 S cm^{-1}, the measured values are in close agreement with the simulated results (gray line), showing a nonlinear increase of SE_T with the increasing conductivity. However, for MXenes with an electrical conductivity of < 100 S cm^{-1}, the measured SE_T values are larger than predicted. This mismatch between the experimental results and theoretical calculations implies that the electrical conductivity is not the only factor responsible for EMI shielding performance of MXenes. On one hand, our theoretical calculations using both the transfer matrix model and Simon's formula do not take into account dielectric polarization effect. The dielectric interactions between the incident EM wave and MXene layers are barely detected for those MXenes with higher conductivity, since the strong interaction between abundant free electrons of highly conductive MXene and incident EM wave dominates the shielding behavior. However, for MXenes with relatively low electrical conductivity, like Nb_2CT_x, the contribution of dielectric interactions between EM wave and the materials to EM wave dissipation is not negligible. MXenes have abundant surface groups and point defects caused by the acid-etching process, as well as adsorbed TMA ions between the layers.[31,32] They may experience strong polarization accompanied with relaxation loss in the altered EM field, contributing to EM wave absorption. On the other hand, both the transfer matrix model and

Simon's formula do not take into account the difference between AC conductivity and DC conductivity for MXenes in the X-band. The frequency-dependent conductivity behavior of different MXenes at gigahertz frequencies is not known, although AC conductivity usually asymptotically approaches the DC conductivity for metals and carbon materials.[33-35] Further investigation is required to quantify the dielectric properties and AC conductivities of MXenes for better understanding of the interaction between EM waves and MXenes. Also, physical models accounting for nanometer-scale heterogeneity of assembled MXene films should be developed.

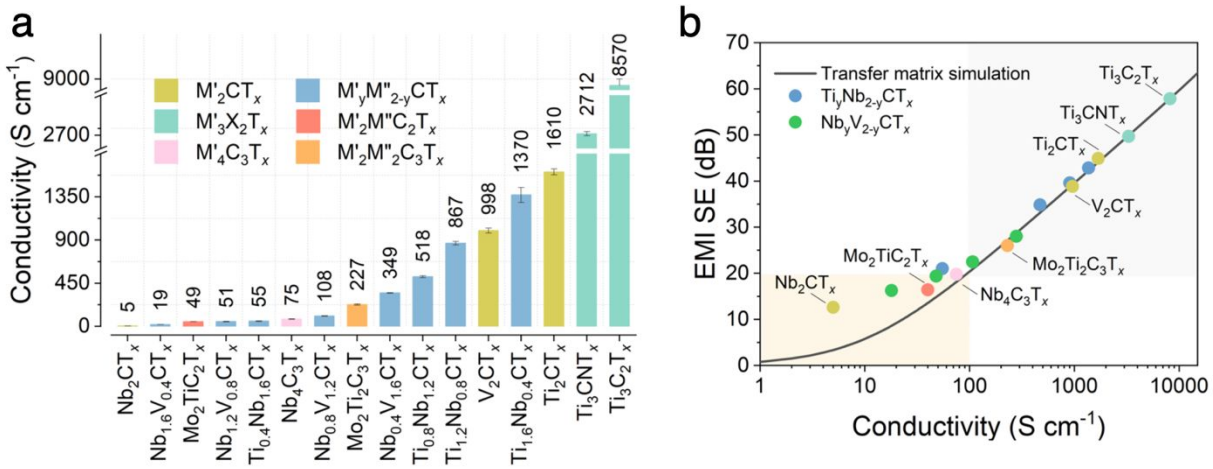

Figure 4. Conductivity-dependent EMI shielding performance of different MXenes. (a) The electrical conductivity of different MXene films. (b) Comparison of EMI SE values between transfer matrix simulation and as-prepared MXene films with a thickness of ~5 μm at 10 GHz, showing the relationship between EMI SE and the electrical conductivity of MXenes.

We have summarized the progress of metal-based hybrids and carbon materials for EMI shielding in recent years, and highlighted the characteristic interval for the MXene films with ~ 2 nm to 15 μm thickness based on the measured EMI shielding properties of different MXenes (details in Table S3). As depicted in Figure 5, it is apparent that most metal-based hybrids and carbon materials require characteristic layer thickness of ~0.1-3 mm to achieve useful EMI SE

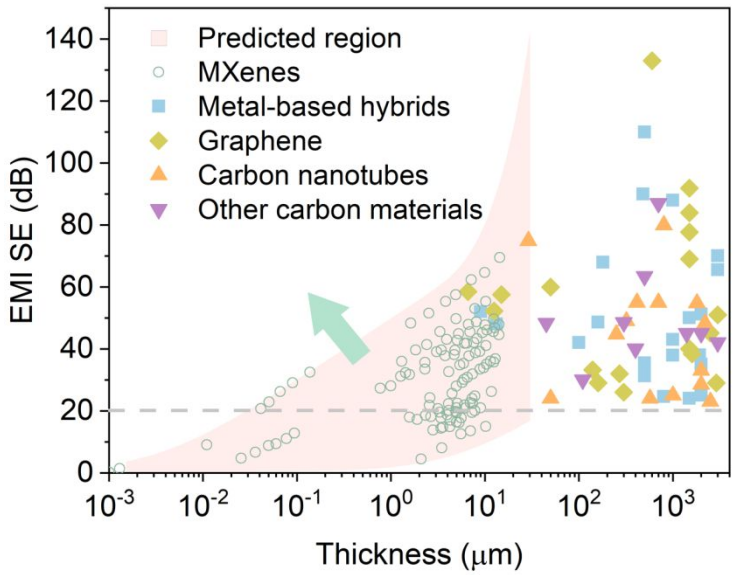

Figure 5. Performance of different materials towards EMI shielding. A comparison of the total EMI SE thickness for the MXene family with metal-based hybrids and carbon materials (graphene, carbon nanotubes, carbon fibers, and others). The gray dashed line is the baseline for the commercial EMI shielding materials (SE_T > 20 dB). A direct comparison of the electrical conductivity and EMI shielding properties of different MXenes with other materials from the literature over the last five years can be found in Table S3.

values, even though some progress has been made in developing thin shielding layers using graphene and metal-based hybrids.[36,37] By contrast, MXenes are effective EMI shields over a broad range of thicknesses, with a minimum thickness of only ~ 40 nm sufficient to achieve 20 dB EMI SE. Furthermore, higher EMI shielding performance can be obtained through further optimization of MAX phase and MXene synthesis, and through modification of the surface chemistry. Many of the MXenes studied in this work were not even previously reported and no optimization of synthesis and conductivity has been done for majority of materials in this study. MXenes not only show superiority with respect to thickness and the feasibility of different coating techniques, but also offer a variety of candidates for manufacturing multifunctional EMI shielding coatings coupled with the optical, mechanical and other properties of different MXenes. It is promising for design of gradient multilayers with tunable EMI shielding properties

using the various combinations of different MXenes. More broadly, the fact that numerous MXenes with different compositions and structures are still unexplored shows the possibility to extend the EMI shielding interval of MXenes towards higher EMI shielding effectiveness and thinner layers.

CONCLUSIONS

In summary, sixteen MXenes with different compositions and M_2XT_x, $M_3X_2T_x$ and $M_4X_3T_x$ structures have been synthesized, delaminated and used to make films of varying thickness. This is the largest set of MXene compositions compared in any single study to date, which demonstrates a wide variety of MXene properties and ways to control them. These samples offer an insight into effects of structure and composition on properties of MXenes. We have showed that the investigated MXene films, ranging from 40 nanometers to several micrometers in thickness, are promising as thin EMI shielding coatings. A transfer matrix model has been shown to fit the EMI shielding performance of MXenes, at least for the most conducting members of the MXene family. Since MXenes have wide variety of useful properties, these results also build a platform for developing multifunctional materials with tunable EMI shielding properties using various MXenes.

METHODS

Materials. For synthesis of the MAX phase precursors, Ti (99.5%, -325 mesh, Alfa Aesar), Al (99.5%, -325 mesh, Alfa Aesar), V (99.5%, -325 mesh, Alfa Aesar), Nb (99.99%, -

325 mesh, Beantown Chemical), AlN (98%, 10 μm, Aldrich), C (graphite, 99%, -325 mesh, Alfa Aesar), TiC (99.5%, typically 2 μm, Alfa Aesar), and Mo (99.9%, -250 mesh, Alfa Aesar) powders were used. For topochemical synthesis to MXene, hydrochloric acid (HCl, 36.5-38%, Fisher Chemical), hydrofluoric acid (HF, 48.5-51%, Acros Organics), lithium chloride (LiCl, 99%, Acros Organics), lithium fluoride (LiF, 98.5%, Alfa Aesar), tetramethylammonium hydroxide (TMAOH, 25 wt%, Acros Organics) were used directly without further purification.

Synthesis of MAX powders. Prior to synthesis, all precursor powders (Table S1, Supporting Information) were mixed with 10 mm zirconia balls in a 2:1 ball : powder ratio. The mixture was placed into plastic jars, then ball milled at 50 rpm for 18 hours. The powder mixture was then transferred to alumina crucibles, which were placed into a high temperature furnace (Carbolite Gero). Ar was flowed through the furnace for 1 h prior to heating, then was continually flowed through the furnace during synthesis. For all samples, the heating rate was 3 °C min^{-1}. Depending on the chemistry and composition, different temperatures and holding times were used (details in Table S1). After cooling, the samples were milled using a TiN-coated milling bit, then were sieved to <75 μm.

Synthesis of MXenes. The synthesis conditions of sixteen MXenes are summarized in Table S2 in Supporting Information. The synthesized procedures in detail for different MXenes are as follows.

Synthesis of $Ti_3C_2T_x$, Ti_2CT_x and Ti_3CNT_x. $Ti_3C_2T_x$, Ti_2CT_x and Ti_3CNT_x were synthesized by the selective etching of the corresponding MAX phase powders (Ti_3AlC_2, Ti_2AlC and Ti_3AlCN) with HF and HCl. Typically, 12 mL of HCl, 2 mL of HF and 6 mL of deionized (DI) water were mixed firstly. After that, 1 g of MAX powder was added to the solution, and

then the mixture kept stirring for 24 h at room temperature. After the etching is done, the reacted solution was centrifuged at 3500 rpm for 2 mins. This washing process was repeated until pH value is >6. The centrifuged sediment was added into a solution of LiCl in DI water with a concentration of 20 mg mL^{-1}. The mixture was stirred for 4 h at room temperature. After that, the solution was centrifuged at 3500 rpm for 10 mins. The centrifugation was repeated until the supernatant became black. The black solution was collected and centrifuged at 7500 rpm for 3 mins. The final supernatant was used for the preparation of MXene films.

Synthesis of $Mo_2TiC_2T_x$ and $Mo_2Ti_2C_3T_x$ and $Nb_4C_3T_x$. $Mo_2TiC_2T_x$ and $Mo_2Ti_2C_3T_x$ and $Nb_4C_3T_x$ were synthesized by the selective etching of the corresponding MAX phase powders (Mo_2TiAlC_2, $Mo_2Ti_2AlC_3$ and Nb_4AlC_3) with HF. Typically, 1 g of MAX phase powder was added into 20 mL of HF with stirring at 50 °C. The etching time for Mo_2TiAlC_2, $Mo_2Ti_2AlC_3$ and Nb_4AlC_3 was 48 h, 96 h and 7 days, respectively. After etching, the reacted solution was washed with DI water through centrifugation (3500 rpm, 2 mins) several times until the pH value is >6. After that, the centrifuged sediment was added into a solution with 0.5 g of TMAOH and 20 mL of DI water, and stirred for 12 h at room temperature. The mixture was centrifuged several times with DI water at 9000 rpm for 10 mins until the pH value is <8. At last, the solution was centrifuged at 3500 rpm for 10 mins. The black supernatant was the dispersion of delaminated MXene flakes in water.

Synthesis of $Ti_yNb_{2-y}CT_x$. $Ti_yNb_{2-y}CT_x$ (y= 0.4, 0.8, 1.2 and 1.6) was synthesized by the selective etching of $Ti_yNb_{2-y}AlC$ powders with a mild method (LiF + HCl). Typically, LiF was dissolved in a mixture of 5mL of DI water and 15 mL of HCl. After that, 1 g of $Ti_yNb_{2-y}AlC$ powder was added to the etchant solution gradually, and stirred for 48 h at 35 °C. Following the reaction, the solution was centrifuged with DI water at 3500 rpm for 2 mins. This washing

procedure was repeated several times until the pH was >6. Finally, the delaminated $Ti_yNb_{2-y}CT_x$ was obtained when the stable black dispersion formed. The supernatant was attained by centrifugation at 7500 rpm for 3 min.

S*ynthesis of* $Nb_yV_{2-y}CT_x$. $Nb_yV_{2-y}CT_x$ (y= 0, 0.4, 0.8, 1.2, 1.6 and 2) was synthesized by the selective etching of the corresponding $Nb_yV_{2-y}AlC$ powders with HF. The etching and delaminated processes are the same as those of $Mo_2TiC_2T_x$ except the etching temperature is 35 °C.

Fabrication of MXene films. The glass slides (24 × 40 × 0.13 mm, Corning, USA) were used as the substrate for spin-casting and spray-coating. Before depositing MXene flakes, the substrates were cleaned with a bath sonication in ethanol and DI water sequentially, and then dried with compressed air. After that, the substrates were cleaned by oxygen plasma with a power of 100 W for 5 mins at a gas flow of 3 sccm.

Spin-casting. The ~2 nm thick MXene films ($Ti_3C_2T_x$ and Ti_2CT_x) were prepared using spin-casting method. Typically, the colloidal solution with a concentration of 1 mg mL^{-1} was spin-cast onto the substrate with spin rate of 1000 rpm for 30 s, followed by 5000 rpm for 10 s.

Spray-coating. The MXene films ($Ti_3C_2T_x$ and Ti_2CT_x) with the thickness of <150 nm were prepared using spray-coating method. Typically, the colloidal solution with a concentration of 1 mg mL^{-1} was sprayed onto the substrate manually. The spray flow was controlled to avoid droplets agglomerating on the substrate. Air flow from a dryer above the substrate provided sufficiently fast drying after each spray.

Vacuum-assistant filtration. The freestanding MXene films were prepared by vacuum-filtering the colloidal MXene dispersion on a polypropylene film with a thickness of 25 μm

(3501 Coated PP, Celgard LLC), and followed by drying in vacuum. The concentration of the colloidal MXene dispersion was calculated based on the weight of the film and the filtered volume of the dispersion.

All films were dried in vacuum oven at 70 °C for 12 h before testing.

Characterization. The morphology and structure of MXene flakes and films were observed using a 3D laser scanning confocal microscopy (Keyence, VK-X1000, Japan), scanning electron microscopy (SEM; Zeiss Supra 50VP, Germany) and transmission electron microscopy (TEM; F-30, FEI-Tecnai, USA). The thickness of MXene flakes was measured by atomic force microscopy (AFM; Multimode 8, Bruker, USA) with a Si tip (Budget Sensors Tap300Al-G; f_0 = 300 kHz, k = 40 N m^{-1}) in a standard tapping mode in air. X-ray diffraction (XRD) patterns were recorded with Ni-filtered Cu Kα radiation (λ = 1.54 Å; Miniflex, Rigaku, USA) operated at 40 kV and 15 mA. The electrical conductivity of MXene films was measured by a four-point probe instrument (ResTest, Jandel Engineering Ltd., Bedfordshire, U.K.) with a probe distance of 1 mm. The thickness of vacuum-filtrated films was measured by a micrometer with 0.1 μm accuracy. UV−vis spectroscopy was performed from 300 to 1000 nm (Evolution 201, Thermo Scientific, 10 mm path length quartz cuvette, USA), and the transmittance value at 550 nm was used to quantify the thickness of the spin-cast and spray-coated films. Scattering parameters of the films were measured using a vector network analyzer (8720ES, Agilent, USA) with a WR-90 rectangular waveguide in the frequency range of 8.2−12.4 GHz.

AUTHOR INFORMATION

Corresponding Author

* Prof. Yury Gogotsi (Y. G.), E-mail: gogotsi@drexel.edu.

ORCID

Meikang Han: 0000-0003-3309-988X

Christopher Eugene Shuck: 0000-0002-1274-8484

Babak Anasori: 0000-0002-1955-253X

Chong Min Koo: 0000-0002-8674-9236

Yury Gogotsi: 0000-0001-9423-4032

Author Contributions

M. H., D. P. and R. R. synthesized MXenes and fabricated MXene films. C. S. and B. A. synthesized MAX phases. M. H. performed the electromagnetic measurement and analyzed the data. G. F. and C. K. contributed to the prediction modelling. M. H. wrote the manuscript, with input from all co-authors. Y. G. initiated the study and supervised the work.

ACKNOWLEDGEMENTS

We thank Dr. Narendra Kurra, Dr. Xu Xiao, and Dr. Mikhail Shekhirev for the MXene film morphology studies, as well as Mark Anayee for computer programming. We are grateful to Murata Manufacturing Co., Ltd, Japan, for providing equipment used for testing EMI shielding properties of MXenes. C. K. acknowledges the financial support from the National Research Foundation of Korea (2017R1A2B3006469 and 2019M3D1A2014004).

SUPPORTING INFORMATION

The Supporting Information is available free of charge at https://pubs.acs.org.

Additional experimental conditions and results, including the tables of synthesis conditions for MAX phases and MXenes; Transfer matrix modeling; XRD patterns of MAX phases and MXenes; Surface morphologies of MXene films; AFM images of MXene flakes; The thickness calculation of MXene films, and corresponding UV-VIS spectra; EMI SE of all MXene films. Table on the comparison of EMI shielding performance of various materials.

REFERENCES

(1) Médard, M., Is 5 Just What Comes after 4? *Nat. Electron.* **2020**, *3*, 2-4.

(2) Huang, W.; Zhou, J.; Froeter, P. J.; Walsh, K.; Liu, S.; Kraman, M. D.; Li, M.; Michaels, J. A.; Sievers, D. J.; Gong, S.; Li, X., Three-Dimensional Radio-Frequency Transformers Based on a Self-Rolled-Up Membrane Platform. *Nat. Electron.* **2018**, *1*, 305-313.

(3) Jiang, Z. Y.; Huang, W.; Chen, L. S.; Liu, Y. H., Ultrathin, Lightweight, and Freestanding Metallic Mesh for Transparent Electromagnetic Interference Shielding. *Opt. Express* **2019**, *27*, 24194-24206.

(4) Wan, Y. J.; Zhu, P. L.; Yu, S. H.; Sun, R.; Wong, C. P.; Liao, W. H., Anticorrosive, Ultralight, and Flexible Carbon-Wrapped Metallic Nanowire Hybrid Sponges for Highly Efficient Electromagnetic Interference Shielding. *Small* **2018**, *14*, 1800534.

(5) Chung, D. D. L., Materials for Electromagnetic Interference Shielding. *J. Mater. Eng. Perform.* **2000**, *9*, 350-354.

(6) Chen, Z.; Xu, C.; Ma, C.; Ren, W.; Cheng, H. M., Lightweight and Flexible Graphene Foam Composites for High-Performance Electromagnetic Interference Shielding. *Adv. Mater.* **2013**, *25*, 1296-1300.

(7) Wei, Q.; Pei, S.; Qian, X.; Liu, H.; Liu, Z.; Zhang, W.; Zhou, T.; Zhang, Z.; Zhang, X.; Cheng, H. M.; Ren, W., Superhigh Electromagnetic Interference Shielding of Ultrathin Aligned Pristine Graphene Nanosheets Film. *Adv. Mater.* DOI: 10.1002/adma.201907411.

(8) Shahzad, F.; Alhabeb, M.; Hatter, C. B.; Anasori, B.; Hong, S. M.; Koo, C. M.; Gogotsi, Y., Electromagnetic Interference Shielding with 2D Transition Metal Carbides (MXenes). *Science* **2016**, *353*, 1137-1140.

(9) Han, M.; Yin, X.; Hantanasirisakul, K.; Li, X.; Iqbal, A.; Hatter, C. B.; Anasori, B.; Koo, C. M.; Torita, T.; Soda, Y.; Zhang, L.; Cheng, L.; Gogotsi, Y., Anisotropic MXene Aerogels with a Mechanically Tunable Ratio of Electromagnetic Wave Reflection to Absorption. *Adv. Opt. Mater.* **2019**, *7*, 1900267.

(10) Yun, T.; Kim, H.; Iqbal, A.; Cho, Y. S.; Lee, G. S.; Kim, M. K.; Kim, S. J.; Kim, D.; Gogotsi, Y.; Kim, S. O., Electromagnetic Shielding of Monolayer MXene Assemblies. *Adv. Mater.*, **2020**, *32*, 2070064.

(11) Wu, X.; Han, B.; Zhang, H. B.; Xie, X.; Tu, T.; Zhang, Y.; Dai, Y.; Yang, R.; Yu, Z. Z., Compressible, Durable and Conductive Polydimethylsiloxane-Coated MXene Foams for High-Performance Electromagnetic Interference Shielding. *Chem. Eng. J.* **2020**, *381*, 122622.

(12) Liu, J.; Zhang, H. B.; Sun, R.; Liu, Y.; Liu, Z.; Zhou, A.; Yu, Z. Z., Hydrophobic, Flexible, and Lightweight MXene Foams for High-Performance Electromagnetic Interference Shielding. *Adv. Mater.* **2017**, *29*, 1702367.

(13) Zhao, S.; Zhang, H. B.; Luo, J. Q.; Wang, Q. W.; Xu, B.; Hong, S.; Yu, Z. Z., Highly Electrically Conductive Three-Dimensional $Ti_3C_2T_x$ MXene/Reduced Graphene Oxide Hybrid

Aerogels with Excellent Electromagnetic Interference Shielding Performances. *ACS Nano* **2018**, *12*, 11193-11202.

(14) Weng, G. M.; Li, J.; Alhabeb, M.; Karpovich, C.; Wang, H.; Lipton, J.; Maleski, K.; Kong, J.; Shaulsky, E.; Elimelech, M.; Gogotsi, Y.; Taylor, A. D., Layer-by-Layer Assembly of Cross-Functional Semi-Transparent MXene-Carbon Nanotubes Composite Films for Next-Generation Electromagnetic Interference Shielding. *Adv. Funct. Mater.* **2018**, *28*, 1803360.

(15) Zhang, C. J.; McKeon, L.; Kremer, M. P.; Park, S. H.; Ronan, O.; Seral Ascaso, A.; Barwich, S.; Coileáin, C. Ó.; McEvoy, N.; Nerl, H. C., Additive-Free MXene Inks and Direct Printing of Micro-Supercapacitors. *Nat. Commun.* **2019**, *10*, 1795.

(16) Sarycheva, A.; Polemi, A.; Liu, Y.; Dandekar, K.; Anasori, B.; Gogotsi, Y., 2D Titanium Carbide (MXene) for Wireless Communication. *Sci. Adv.* **2018**, *4*, eaau0920.

(17) Salles, P.; Pinto, D.; Hantanasirisakul, K.; Maleski, K.; Shuck, C. E.; Gogotsi, Y., Electrochromic Effect in Titanium Carbide MXene Thin Films Produced by Dip-Coating. *Adv. Funct. Mater.* **2019**, *29*, 1809223.

(18) Kim, S. J.; Choi, J.; Maleski, K.; Hantanasirisakul, K.; Jung, H. T.; Gogotsi, Y.; Ahn, C. W., Interfacial Assembly of Ultrathin, Functional MXene Films. *ACS Appl. Mater. Interfaces* **2019**, *11*, 32320-32327.

(19) Anasori, B.; Lukatskaya, M. R.; Gogotsi, Y., 2D Metal Carbides and Nitrides (MXenes) for Energy Storage. *Nat. Rev. Mater.* **2017**, *2*, 16098.

(20) Deysher, G.; Shuck, C. E.; Hantanasirisakul, K.; Frey, N. C.; Foucher, A. C.; Maleski, K.; Sarycheva, A.; Shenoy, V. B.; Stach, E. A.; Anasori, B.; Gogotsi, Y., Synthesis of

Mo_4VAlC_4 MAX Phase and Two-Dimensional Mo_4VC_4 MXene with 5 Atomic Layers of Transition Metals. *ACS Nano* **2020**, *14*, 204-217.

(21) Sokol, M.; Natu, V.; Kota, S.; Barsoum, M. W., On the Chemical Diversity of the MAX Phases. *Trends Chem.* **2019**, *1*, 210-223.

(22) Anasori, B.; Gogotsi, Y., *2D Metal Carbides and Nitrides (MXenes)*. Springer: Berlin, **2019**; pp 15-19.

(23) Maleski, K.; Mochalin, V. N.; Gogotsi, Y., Dispersions of Two-Dimensional Titanium Carbide MXene in Organic Solvents. *Chem. Mater.* **2017**, *29*, 1632-1640.

(24) Hantanasirisakul, K.; Gogotsi, Y., Electronic and Optical Properties of 2D Transition Metal Carbides and Nitrides (MXenes). *Adv. Mater.* **2018**, *30*, 1804779.

(25) Anasori, B.; Xie, Y.; Beidaghi, M.; Lu, J.; Hosler, B. C.; Hultman, L.; Kent, P. R. C.; Gogotsi, Y.; Barsoum, M. W., Two-Dimensional, Ordered, Double Transition Metals Carbides (MXenes). *ACS Nano* **2015**, *9*, 9507-9516.

(26) Seredych, M.; Shuck, C. E.; Pinto, D.; Alhabeb, M.; Precetti, E.; Deysher, G.; Anasori, B.; Kurra, N.; Gogotsi, Y., High-Temperature Behavior and Surface Chemistry of Carbide MXenes Studied by Thermal Analysis. *Chem. Mater.* **2019**, *31*, 3324-3332.

(27) Simon, R. M., EMI Shielding through Conductive Plastics. *Polym. Plast. Technol. Eng.* **1981**, *17*, 1-10.

(28) Yang, Y.; Zhu, D.; Yan, W.; Agarwal, A.; Zheng, M.; Joannopoulos, J. D.; Lalanne, P.; Christensen, T.; Berggren, K. K.; Soljačić, M., A General Theoretical and Experimental Framework for Nanoscale Electromagnetism. *Nature* **2019**, *576*, 248-252.

(29) Dillon, A. D.; Ghidiu, M. J.; Krick, A. L.; Griggs, J.; May, S. J.; Gogotsi, Y.; Barsoum, M. W.; Fafarman, A. T., Highly Conductive Optical Quality Solution-Processed Films of 2D Titanium Carbide. *Adv. Funct. Mater.* **2016**, *26*, 4162-4168.

(30) Ying, G.; Dillon, A. D.; Fafarman, A. T.; Barsoum, M. W., Transparent, Conductive Solution Processed Spincast 2D Ti_2CT_x (MXene) Films. *Mater. Res. Lett.* **2017**, *5*, 391-398.

(31) Watts, P. C. P.; Hsu, W. K.; Barnes, A.; Chambers, B., High Permittivity from Defective Multiwalled Carbon Nanotubes in the X-Band. *Adv. Mater.* **2003**, *15*, 600-603.

(32) Yin, X.; Kong, L.; Zhang, L.; Cheng, L.; Travitzky, N.; Greil, P., Electromagnetic Properties of Si–C–N Based Ceramics and Composites. *Int. Mater. Rev.* **2014**, *59*, 326-355.

(33) Al-Saleh, M. H.; Saadeh, W. H.; Sundararaj, U., EMI Shielding Effectiveness of Carbon Based Nanostructured Polymeric Materials: A Comparative Study. *Carbon* **2013**, *60*, 146-156.

(34) Naishadham, K.; Kadaba, P. K., Measurement of the Microwave Conductivity of a Polymeric Material with Potential Applications in Absorbers and Shielding. *IEEE Trans. Microw. Theory Tech.* **1991**, *39*, 1158-1164.

(35) Awan, S.; Lombardo, A.; Colli, A.; Privitera, G.; Kulmala, T.; Kivioja, J.; Koshino, M.; Ferrari, A., Transport Conductivity of Graphene at RF and Microwave Frequencies. *2D Mater.* **2016**, *3*, 015010.

(36) Wang, Z.; Mao, B.; Wang, Q.; Yu, J.; Dai, J.; Song, R.; Pu, Z.; He, D.; Wu, Z.; Mu, S., Ultrahigh Conductive Copper/Large Flake Size Graphene Heterostructure Thin Film with Remarkable Electromagnetic Interference Shielding Effectiveness. *Small* **2018**, *14*, 1704332.

(37) Lin, S.; Ju, S.; Shi, G.; Zhang, J.; He, Y.; Jiang, D., Ultrathin Nitrogen-Doping Graphene Films for Flexible and Stretchable EMI Shielding Materials. *J. Mater. Sci.* **2019**, *54*, 7165-7179.

TABLE OF CONTENTS GRAPHIC